

QCD with two light dynamical chirally improved quarks: MesonsGeorg P. Engel,¹ C. B. Lang,¹ Markus Limmer,¹ Daniel Mohler,^{1,2} and Andreas Schäfer³

(BGR [Bern-Graz-Regensburg] Collaboration)

¹*Institut für Physik, FB Theoretische Physik, Universität Graz, A-8010 Graz, Austria*²*TRIUMF, 4004 Wesbrook Mall Vancouver, BC V6T 2A3, Canada*³*Institut für Theoretische Physik, Universität Regensburg, D-93040 Regensburg, Germany*

(Received 13 December 2011; published 28 February 2012)

We present results for the spectrum of light and strange mesons on configurations with two flavors of mass-degenerate Chirally Improved sea quarks. The calculations are performed on seven ensembles of lattice size $16^3 \times 32$ at three different gauge couplings and with pion masses ranging from 250 to 600 MeV. To reliably extract excited states, we use the variational method with an interpolator basis containing both Gaussian and derivative quark sources. Both conventional and exotic channels up to spin 2 are considered. Strange quarks are treated within the partially quenched approximation. For kaons we investigate the mixing of interpolating fields corresponding to definite C -parity in the $SU(3)$ limit. This enlarged basis allows for an improved determination of the low-lying kaon spectrum. In addition to masses we also extract the ratio of the pseudoscalar decay constants of the kaon and pion and obtain $F_K/F_\pi = 1.215(41)$. The results presented here include some ensembles from previous publications and the corresponding results supersede the previously published values.

DOI: [10.1103/PhysRevD.85.034508](https://doi.org/10.1103/PhysRevD.85.034508)

PACS numbers: 12.38.Gc, 11.15.Ha

I. INTRODUCTION

Considering only strong decays, with the exception of the pion and the proton all hadrons are resonances, embedded in a continuous spectrum. In lattice calculations we can only determine discrete energy levels, with spacings $\mathcal{O}(1/L)$ related to the spatial extent L of the studied lattice volume. When disregarding the fermion vacuum in the so-called quenched simulations energy levels can be related directly to hadron excitations. In dynamical situations the energy levels are denser close to resonances and they are influenced by coupled open hadronic scattering channels. Although in principle the Euclidean correlator of any hadron interpolator with the correct quantum numbers should feel these scattering channels, in actual calculations there is little, if any, trace of it [1,2] unless such multi-hadron interpolators are included explicitly in the set of operators. However, inclusion of those is costly, since it involves disconnected contributions. In actual calculations efficient but demanding all-to-all propagator methods are used [3–7].

In recent years much effort has been invested into developing methods for determining the lowest energy levels for hadron correlators. In [1,2,8–13] meson excitations have been studied in a dynamical quark background with a variety of quarks species, interpolators, and extraction methods. A central technique employed was the variational method [14,15] where one finds the energy levels by diagonalization of cross correlations of a (hopefully) sufficiently large set of interpolators which allows for a good overlap with the relevant hadron states.

In continuum quantum field theory there has been recent progress in investigations of mesons using Schwinger-Dyson equations and the Bethe-Salpeter equation as well as effective field theories (see, for example, Refs. [16–22]).

Starting with [23], we have been determining hadron ground states and low excited states in a framework of simulations with two light dynamical quarks. The fermionic action used is the so-called Chirally Improved (CI) action [24,25], an approximate solution to the Ginsparg-Wilson relation for fermions obeying chiral symmetry in a lattice form. The strange quarks have been incorporated in the valence sector only. In [1] results based on three ensembles at three different gauge couplings but with only one quark mass for each coupling have been presented. We have meanwhile significantly extended the statistics and also the number of ensembles. Here, we present our results for the meson sector based on the final set of seven ensembles at three gauge couplings and two or three quark mass values at each. This allows an extrapolation towards the physical point. Previously published results are generally confirmed, although in some cases we observe new behavior related to new symmetry considerations. Some results have been presented already in [26].

Following the presentation of the action and the parameters of the gauge configuration ensembles in Sec. II, we discuss scale setting, decay constants, and the quark mass in Sec. III. The interpolators used for the meson fields in the variational analysis are discussed in Sec. IV and tabulated in the Appendix. The main parts are Secs. V and VI, where results for the mesons are presented.

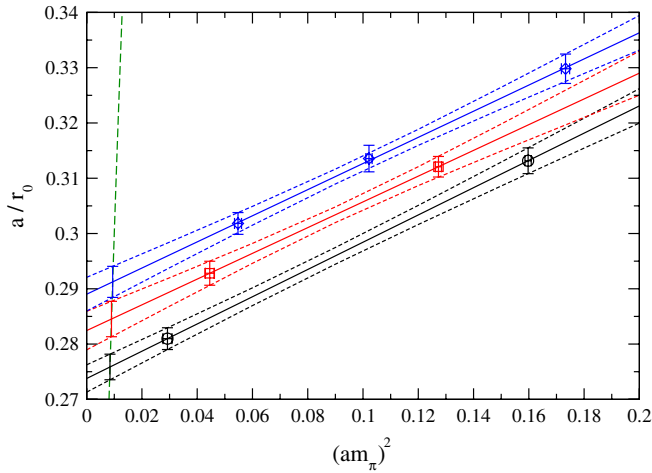


FIG. 1 (color online). Setting the scale with the Sommer parameter and the pion mass as input at the physical point. The green (long-dashed) line is the curve Eq. (2). The solid and short-dashed lines represent the extrapolation of our lattice data. Their intersections with the green line define the lattice constants a .

II. ACTION AND SIMULATION

A. Fermion action and gauge action

In our study the fermions are represented by the Chirally Improved Dirac operator D_{CI} [24,25]. This is an approximate solution of the Ginsparg-Wilson equation and results from a general ansatz for the Dirac operator, namely, an expansion of the form

$$D = m_0 \mathbb{1} + D_{\text{CI}}, \quad D_{\text{CI}}(n, m) = \sum_{i=1}^{16} c_{nm}^{(i)}(U) \Gamma_i, \quad (1)$$

where the sum runs over all 16 elements Γ_i of the Clifford algebra and the coefficients $c_{nm}^{(i)}$ were fit by minimizing the violation of the Ginsparg-Wilson equation. It includes paths up to a maximum length of 4 lattice units. The paths and coefficients used are found in the appendix of [23]. We used the same 19 coefficients for all ensembles, modifying only the diagonal mass term in order to account for the additive mass renormalization. For that reason the values of the bare mass parameter m_0 given in Table I are negative. Thus, the actual (unrenormalized) mass is given by the values m_{AWI} determined from the axial Ward identity.

For further improvement of the fermion action one level of stout smearing of the gauge fields [27] was included in its definition. The parameters are adjusted such that the value of the plaquette is maximized ($\rho = 0.165$ following [27]). For the pure gauge field part of the action we use the tadpole-improved Lüscher-Weisz gauge action [28]. For a given gauge coupling we used the same assumed plaquette value for the different values of the bare quark mass parameter.

B. Lattice ensembles

The analysis presented here is based on seven ensembles of configurations for lattice size $16^3 \times 32$. These substantially extend (by a factor of 3) the data base of [1,23]. A summary of the notation and some parameters of these ensembles is given in Table I.

The notation for the couplings follows [23], where all parameters of the fermion action are detailed. For each value of the gauge coupling we have two or three values of the quark mass parameter. Following equilibration every 5th configuration has been selected for analysis. Further details on the updating hybrid Monte Carlo algorithm and statistical checks for equilibration have been discussed in [23].

From the values of $m_\pi L$ we expect non-negligible finite size effects for the three ensembles with smallest quark mass, A66, B70, and C77. Discretization effects have been discussed in the quenched simulations, where for the used action only small $\mathcal{O}(a^2)$ corrections have been identified [29]. In order to confirm this for the dynamical simulation we would have to perform our study at several lattice spacings and volumes, which is not possible based on the given ensembles and statistics. Studies with a larger volume ($24^3 \times 48$) with linear size $\mathcal{O}(3.6 \text{ fm})$ are in progress.

III. SCALE AND LOW ENERGY PARAMETERS

A. Scale

In our earlier work [1,23] we had analyzed configurations at one quark mass parameter for three values of the gauge coupling. There, we used the lattice spacing derived from the static potential with a Sommer parameter $r_0 = 0.48 \text{ fm}$. Now we have two or three quark mass parameters for each gauge coupling and can attempt an extrapolation to the physical point or the chiral limit. The latter extrapolation would be relevant for the parameters of chiral perturbation theory, which we will not attempt to extract here.

We use two approaches to set the scale. In the first one we determine $y \equiv a/r_0$ from the static potential separately

TABLE I. Parameters of the simulation: We used several ensembles with different gauge couplings β_{LW} and/or light quark mass parameters $m = 0$. We also show the strange quark mass parameter m_s , the number of configurations analyzed, and the physical extent of the spatial volume multiplied with the pion mass.

Set	β_{LW}	m_0	m_s	Configurations	$m_\pi L$
A50	4.70	-0.050	-0.020	200	6.4
A66	4.70	-0.066	-0.012	200	2.7
B60	4.65	-0.060	-0.015	300	5.7
B70	4.65	-0.070	-0.011	200	3.4
C64	4.58	-0.064	-0.020	200	6.7
C72	4.58	-0.072	-0.019	200	5.1
C77	4.58	-0.077	-0.022	300	3.7

TABLE II. Lattice spacing in physical units derived for ensembles of types A, B, and C (cf. Table I) by the methods discussed in the text.

	A	B	C
$(\pi, r_0)_{\text{phys}}$	0.1324(11)	0.1366(15)	0.1398(14)
$(\pi, r_0)_{\text{chiral}}$	0.1314(12)	0.1356(17)	0.1387(15)
$(\pi, \rho)_{\text{phys}}$	0.1330(44)	0.1378(50)	0.1400(29)

for each ensemble, as discussed in [23]. We then study the dependence of this quantity on the measured values of $x \equiv (am_\pi)^2$ (cf. Fig. 1). The physical values are obtained along

$$y = \frac{\sqrt{x}}{m_\pi r_0}. \quad (2)$$

For each of the three gauge couplings we then perform a linear fit and obtain the physical value where the extrapolations intersect Eq. (2) with $m_\pi r_0 = 137 \text{ MeV} \times 0.48 \text{ fm} = 0.3332$. (We use the average of charged and neutral pion masses.) From this one reads off the lattice spacing a . Table II gives the resulting value in the row labeled $(\pi, r_0)_{\text{phys}}$. The value in the chiral limit is obtained as usual from a/r_0 where $am_\pi = 0$.

The other approach is to replace $y = a/r_0$ by mass values like am_N or am_ρ . Since the ρ is unstable for small enough pion mass, there will be threshold effects. In our parameter range we find no coupling to the (p-wave) $\pi\pi$ sector yet and a linear extrapolation intersecting with $y = \sqrt{x}m_\rho/m_\pi$ gives the values of the lattice spacing in Table II compatible with the results of the first method, but with larger errors.

Throughout this presentation we will use the values obtained from the definition denoted by $(\pi, r_0)_{\text{phys}}$ in Table II.

B. Setting the strange quark mass

In this two-flavor simulation we use the partial quenching approximation to access the strange hadron spectrum, i.e., we consider the strange quark as a valence quark only. In view of results with full strange quark dynamics (e.g., [30]) we find, at least for the ground states, no noticeable difference in the mass range considered here.

In each ensemble the strange quark mass parameter m_s is set by identifying our result for the Ω baryon positive parity ground state energy level with the physical $\Omega(1672)$. These parameters are found in Table I.

For this definition we use $r_{0,\text{exp}} = 0.48 \text{ fm}$ in each ensemble, differing from the (in Sec. III A) discussed method to set the overall scale. Since the two different definitions agree at physical pion masses, this method is consistent at the physical point, but results have to be taken with care at unphysically large pion masses.

C. AWI mass

The so-called axial Ward identity (AWI) mass (or PCAC mass) is determined from the asymptotic (i.e., plateau of the) ratio of the unrenormalized correlators,

$$2m_{\text{AWI}} = \frac{c_A}{c_P} \frac{\langle 0 | \partial_t A_4^+(p=0, t) X(0) | 0 \rangle}{\langle 0 | P^-(p=0, t) X(0) | 0 \rangle}, \quad (3)$$

where $P^- = \bar{d}\gamma_5 u$, $A_4^- = \bar{d}\gamma_4\gamma_5 u$, and X is an interpolator with the quantum numbers of the pion, usually P^+ or A^+ . The constants $c_A(s)$ and $c_P(s)$ denote the lattice factors relating the smeared interpolators to the lattice pointlike interpolators (not to be confused with the renormalization constants Z relating lattice point operators to the continuum renormalization scheme). They are obtained from the ratio of correlators from smeared to point sources [23].

The relation to the renormalized quark mass needs the renormalization factors for the pseudoscalar and axial currents,

$$m^{(r)} = \frac{Z_A}{Z_P} m_{\text{AWI}}. \quad (4)$$

Table III gives the values of m_{AWI} and m_π for the ensembles studies. (Values for the renormalization constants have been derived in [31,32].)

D. Decay constants

The pseudoscalar decay constant describes the coupling to weak decays. It can be extracted from the asymptotic behavior of the correlation between the pseudoscalar or the time components of the axial interpolators,

$$c_A^2 Z_A^2 \langle A_4^-(p=0, t) A_4^+(0) \rangle \sim m_\pi F_\pi^2 e^{-m_\pi t} \equiv c e^{-m_\pi t}. \quad (5)$$

TABLE III. Pion masses and quark AWI masses for the different sets of gauge configurations.

Set	a [fm]	am_π	m_π [MeV]	am_{AWI}	m_{AWI} [MeV]
A50	0.1324(11)	0.3997(14)	596(5)	0.030 27(8)	45(1)
A66	0.1324(11)	0.1710(48)	255(7)	0.005 89(40)	9(1)
B60	0.1366(15)	0.3568(15)	516(6)	0.023 56(13)	34(1)
B70	0.1366(15)	0.2111(38)	305(6)	0.008 36(23)	12(1)
C64	0.1398(14)	0.4163(18)	588(6)	0.029 95(20)	42(1)
C72	0.1398(14)	0.3196(18)	451(5)	0.017 28(16)	24(1)
C77	0.1398(14)	0.2340(27)	330(5)	0.010 54(19)	15(1)

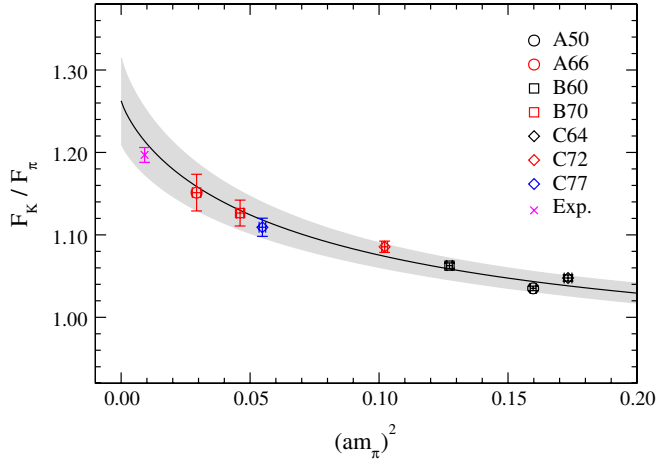


FIG. 2 (color online). The ratio of F_K/F_π is plotted against m_π^2 (in dimensionless units) for each set of gauge configurations. The full black line is a fit of the data using the relevant expressions for numerator and denominator; the shaded area indicates the error band. The magenta cross indicates the experimental value [36].

The coefficient then gives

$$F_\pi = 2m_{\text{AWI}}c_P Z_A \sqrt{\frac{c}{m_\pi^3}}, \quad (6)$$

and equivalently for the kaon F_K .

The dependence of the pion decay constant on the quark mass can be described by chiral perturbation theory. Up to 1-loop order, one finds [33]

$$F_\pi = F_{\pi,0} - m \frac{2\Sigma_0}{16\pi^2 F_{\pi,0}^3} \ln\left(m \frac{2\Sigma_0}{\Lambda_4^2 F_{\pi,0}^2}\right). \quad (7)$$

Here, $F_{\pi,0}$ and Σ_0 refer to the pion decay constant and the quark condensate in the chiral limit $m \rightarrow 0$ and Λ_4 is a low energy constant. The corresponding expressions including the 2-loop order can be found in [34,35].

The renormalization factor Z_A cancels in the ratio F_K/F_π . We show this ratio in Fig. 2 where we assume a lattice spacing of 0.135 fm [the average of our values for the scheme $(\pi, r_0)_{\text{phys}}$] and a physical pion mass of 139.57 MeV. The extrapolation of our data to that point gives

$$F_K/F_\pi = 1.215(41), \quad (8)$$

which fully covers the experimental value 1.197(9) [36].

IV. ANALYSIS METHOD AND MESON INTERPOLATORS

Given interpolating operators O_M with the quantum numbers of a hadron, the correlation function of such operators separated by some Euclidean time distance provides the energy spectrum,

$$\langle O_M(t) O_M^\dagger(0) \rangle = \sum_n \langle O_M | n \rangle \langle n | O_M^\dagger \rangle e^{-E_n t}. \quad (9)$$

The asymptotic exponential decay, however, gives just the ground state energy in that channel. On finite lattices, depending on parameters like size and lattice spacing, this may be related either to a single meson or to meson scattering states. For the study of scattering and of higher lying mesons it is imperative to find also the excited energy levels.

An efficient tool for this is the so-called variational analysis [14,15,37]. Using several interpolators with the correct quantum numbers, one diagonalizes the cross-correlation matrix of these, using the generalized eigenvalue formulation

$$\begin{aligned} C_{ij}(t) &\equiv \langle O_i(t) O_j^\dagger(0) \rangle, \\ C(t) \vec{v}_k(t, t_0) &= \lambda_k(t, t_0) C(t_0) \vec{v}_k(t, t_0). \end{aligned} \quad (10)$$

If the set of interpolators is large enough, then one expects that the eigenvectors approach the eigenstates of the system. In fact, the eigenvectors act as a fingerprint of the states and should remain stable over the considered window of t values. In such a window the eigenvalues decay exponentially, approximating the desired eigenenergies,

$$\lambda_k(t, t_0) \propto e^{-(t-t_0)E_k} (1 + \mathcal{O}(e^{-(t-t_0)\Delta E_k})). \quad (11)$$

Here, depending on t and t_0 , the value of ΔE_k denotes either the difference to the first neglected energy level (for $t_0 \leq t \leq 2t_0$) or to the nearest energy level (for a careful discussion see [37]). It was also demonstrated that even ghost states can be identified with this type of analysis [38].

A possible systematic influence comes from choosing t_0 in the variational method and the fit range for the generalized eigenvalues. We use $t_0 = 1$ throughout. In principle, the impact of that choice can be estimated by choosing several values of t_0 and varying the fit range. For the final fit, one should then choose a window where this impact is negligible. However, in practice the corresponding choices are restricted by the given signal-to-noise ratio for coarse lattices and weak signals. In the actual analysis, one determines the window from a combination of indicators, ranging from effective energy values to approximate constancy of the corresponding eigenvectors. The energy levels then result from an exponential fit to the eigenvalues over that window. In some cases a second exponential is used in these fits to allow for a small admixture of higher energy states.

Various techniques have been suggested to construct interpolators. In [39] we introduced lattice operators based on smeared quarks. Combining differently smeared quarks,

also including covariant derivatives [40–42], several meson and baryon energy levels could be determined in the quenched [43,44] and dynamical case [1].

The interpolators are constructed by hypercubic smearing [45–47] the time slice gauge variables, i.e., smearing only the spatial links in each time slice.¹ Based on these gauge variables the quark sources are smeared with the covariant Jabobi smearing [48,49],

$$S_{\kappa,K} = \sum_{n=0}^K \kappa^n H^n S_0, \quad (12)$$

$$H(\vec{n}, \vec{m}) = \sum_{j=1}^3 (U_j(\vec{n}, 0) \delta(\vec{n} + \hat{j}, \vec{m}) + U_j(\vec{n} - \hat{j}, 0)^\dagger \delta(\vec{n} - \hat{j}, \vec{m})), \quad (13)$$

where S_0 denotes the point source. The parameters K and κ are adjusted to obtain Gaussian-like shapes of the sources [44] with different smearing widths. In the definitions of the operators we denote the smearing types by n and w (narrow and wide) and by ∂_k for the derivative in spatial direction k . The widths of the sources do not exactly agree for the various ensembles (which would be dependent on the definition of the scale anyway.) However, the width of the narrow source is in the range 0.2 to 0.3 fm and the width of the wide source is in the range 0.4 to 0.6 fm.

The derivative sources S_{∂_k} have been constructed numerically by applying the covariant difference operators on the wide source, S_w , see [42,50]. This corresponds to an asymmetric definition of the interpolators. If S^1, S_2 denote Gaussian smearing operators and \vec{D} the derivative acting to the right, then our operators (involving one derivative) have the structure

$$O = \bar{\psi}(S^1 \Gamma S^2 \vec{D} \pm \vec{D} S^2 \Gamma S^1) \psi \quad (14)$$

instead of

$$O = \bar{\psi}(S^1 \Gamma \vec{D} S^2 \pm S^2 \vec{D} \Gamma S^1) \psi, \quad (15)$$

where the “ \pm ” symmetrization ensures a good C -parity quantum number. Following Eq. (15), some interpolators (with $S^1 = S^2$) are identical to zero after partial integration. The operator Eq. (14) is in general nonvanishing even if $S^1 = S^2$, since $[D, S] \neq 0$. This commutator can be seen as introducing additional pieces of paths in the combined smearing operator, which means changed weights of the existing paths and a few new paths. Numerically, we find

¹Notice that the Dirac operator already contains one level of stout smearing. We use these stout smeared gauge links and apply additional smearing to construct the sources.

that the corresponding correlators are of the same magnitude as others and yield consistent signals. Hence, this asymmetric definition enlarges effectively the basis of operators to some extent. In particular, some exotic channels can be accessed this way already with fewer derivatives.

In the Appendix we list all meson interpolators used in our study, ordered according to their spin and parity (Tables IV, V, VI, VII, VIII, IX, X, and XI). The tables differ from those in [1] since we here account for the approximate symmetry under C -parity of strange mesons and construct the interpolators accordingly. Monitoring the eigenvectors in the variational method allows for insights in approximate C -parities of various strange meson states, and furthermore in the breaking of C -parity of strange mesons when approaching the physical pion mass.

V. ISOVECTOR LIGHT MESONS

The energy levels are obtained from exponential fits to the eigenvalues in a range of t values where the eigenvalues and eigenvectors are compatible with plateau behavior. Typically that plateau extends from $t = 2$ or 3 up to $t = 6$ to 12. In some cases the eigenvalues are close to each other and their order changes from one time slice to another and also changes randomly over the set of configurations. This complicates the exponential fits to the eigenvalues and the automatic attribution of the eigenvectors to physical eigenstates. In such situations we use scalar products of eigenvectors at a given time slice with the eigenvectors at the preceding time slice to sort the eigenvalues according to their corresponding physical states. This procedure becomes more reliable towards finer lattice spacings. For subsets of configurations (in the jackknife analysis), the eigenvectors are contracted with the average of the vectors at the same time slice.

All masses are extrapolated towards the physical point as a function of the pion ground state mass squared. In the plots we also show the corresponding one σ error band (dashed curves). The number of energy levels shown is always less than the number of interpolators chosen for the diagonalization. The χ^2 per degree of freedom for the chiral fits of all energy levels are collected in Tables XII, XIII, and XIV.

A. Scalars

$0^{-+}(\pi)$: For the first excitation in the pion channel (see Fig. 3), the set of operators (1, 2, 17) is used in all ensembles. The corresponding effective mass plateaus are rather short, increasing the uncertainty of the extracted mass. Because of the finiteness of the lattice, the back-running pion limits the possible fit range for the first excitation [23,42,51], in particular, at small pion masses.

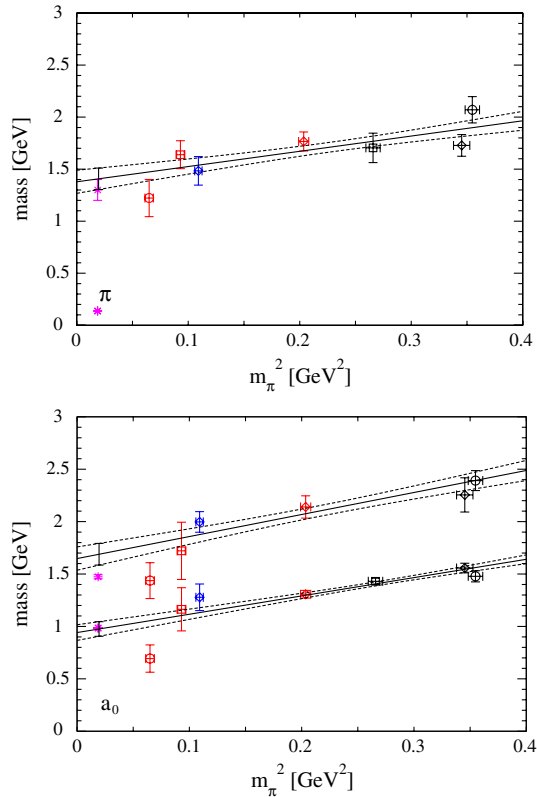


FIG. 3 (color online). 0^{-+} (top): Only the first excitation is shown, the ground state pion mass squared defines the abscissa. 0^{++} (bottom): Observed ground state and first excitation.

Nevertheless, masses can be extracted and the chiral extrapolation hits the experimental $\pi(1300)$ within 1σ .

$0^{++}(a_0)$: In [1], three (A50, B70, and C77) of the seven ensembles have been analyzed, with less statistics than in the present work. Partially quenched data was used to argue that the signal in the 0^{++} channel probably has significant contributions from the S-wave scattering state $\pi\eta_2$. In the present work we analyze only fully dynamical data (except for the strange sector). Our results are now compatible with the experimental ground state $a(980)$ within 1σ and with the first excitation $a(1450)$ within 2σ (see Fig. 3). However, the channel still poses some difficulties. The plateau is rather short and there remains some ambiguity in choosing the fit range, leading to a systematic error. In addition, the results depend on the chosen set of interpolators. We show results from subsets of (1, 4, 10, 12, 13). In ensemble B60, the excitation signal was not good enough to be fitted. The extrapolations of the ground state levels agree for the different choices of interpolators.

However, in particular the ground state energy level of ensemble A66 deviates when changing the set of interpolators. The result becomes unexpectedly light, most pronounced in the case of the set (10, 12, 13), though the corresponding effective mass plateaus look stable. Indeed, this point lies below the (theoretical) $\pi\eta_2$ threshold and

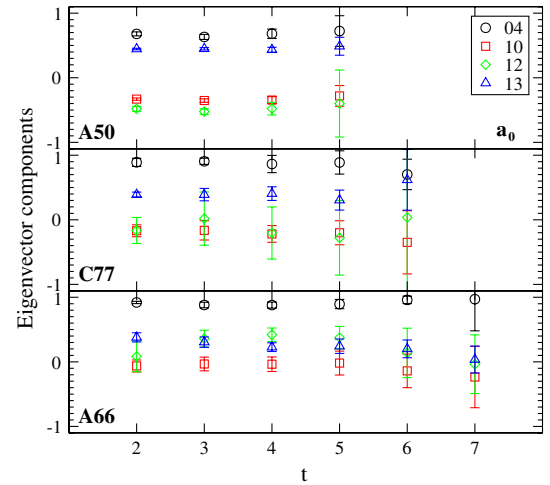


FIG. 4 (color online). Eigenvector components of the ground state of the light scalar meson channel (a_0) of ensembles A50, C77, and A66 (top to bottom). Interpolator (4) (only Gaussian sources) dominates, while contributions of the other interpolators (one or two derivatives) is found to be particularly relevant at heavy pions. Nevertheless, the eigenvectors are very similar over the whole range of pion masses (600 to 250 MeV) and only evolve smoothly.

could indicate a scattering state signal. It also could signal a severe finite size effect for this case in A66; this could be clarified only by increasing the lattice volume. Nevertheless, except for this point, the results are compatible with the experimental states.

In Fig. 4 we show the eigenvectors for the ground state for three ensembles covering the whole range of pion masses presented. They are quite consistent with each other and not supporting the notion of a change in the physics of the ground state over that range. Figure 5 shows the effective masses of ground state and first excited energy level for the ensemble with smallest pion mass (A66).

There are studies for the finite size dependence of the lowest energy level in this channel based on unitarized chiral perturbation theory [21]. However, at the moment our values are not precise enough to decide on these grounds on properties of the a_0 . Also it may be necessary

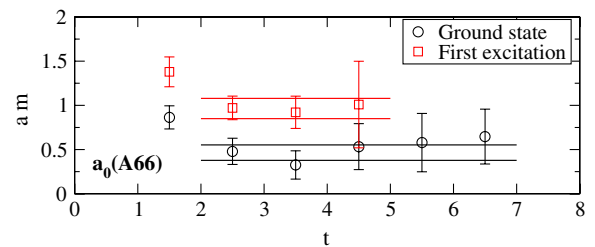


FIG. 5 (color online). Effective mass plateaus for the light scalar meson channel (a_0) of ensemble A66, ground state and first excitation.

to include meson-meson interpolators in a more detailed study. Simulations to address finite size effects are currently in progress and the discussion of this ongoing effort is beyond the scope of the current publication.

B. Vectors

$1^{--}(\rho)$: The $\rho(770)$ comes out nicely as usual (see Fig. 6). The first and second excitation are extracted using the set (1, 8, 12, 17, 22), where the second excitation is not stable in A66. These excitations are very close to one another, making the chiral extrapolations less reliable. The pattern of energy levels would allow a crossover of eigenstates but the eigenvectors do not confirm this. Therefore, we extrapolate the results to the physical point according to the naively assumed level ordering, neglecting a possible crossover. The results are compatible with the experimental $\rho(1450)$ and $\rho(1570$ or $1700)$ within error bars (for a discussion on the latter excitation see [36]).

We find no obvious indication for a coupled $\pi\pi$ P-wave channel. As discussed earlier [1,52] this may be due to weak coupling. By including two pion interpolators, one can derive a scattering phase shift from the modification of the observed energy levels close to the resonance (see, e.g.

[53]). Such a study needs inclusions of disconnected graphs, which are not accessible to us: The necessary propagator calculation is numerically too costly for CI fermions.

$1^{-+}(\pi_1)$: The quantum numbers 1^{-+} cannot be obtained with isotropic quark sources only. Thus, this channel is not accessible by simple quark models, and it is commonly referred to as exotic. Because of the weak signal, the set of operators has to be optimized in each ensemble separately, taking one or two interpolators of (9, 11, 14, 16, 21, 24). This way a mass value can be extracted only with comparatively large statistical uncertainty. The chiral extrapolation hits the experimental $\pi_1(1400)$, but is also compatible with the $\pi_1(1600)$ (see Fig. 6). In some of the ensembles we get the best signal using interpolators which are nonzero only due to the definition in Eq. (14) and discussed there. This may be related to the “exotic” property of this channel.

$1^{++}(\mathbf{a}_1)$: The signal in the pseudovector meson channels is usually bad compared to the pion and the ρ channels. Nevertheless, the ground state and a first excitation can be identified. The ground state is extracted using the single interpolator (1). For the first excitation the set has to be optimized in each ensemble separately, taking subsets of

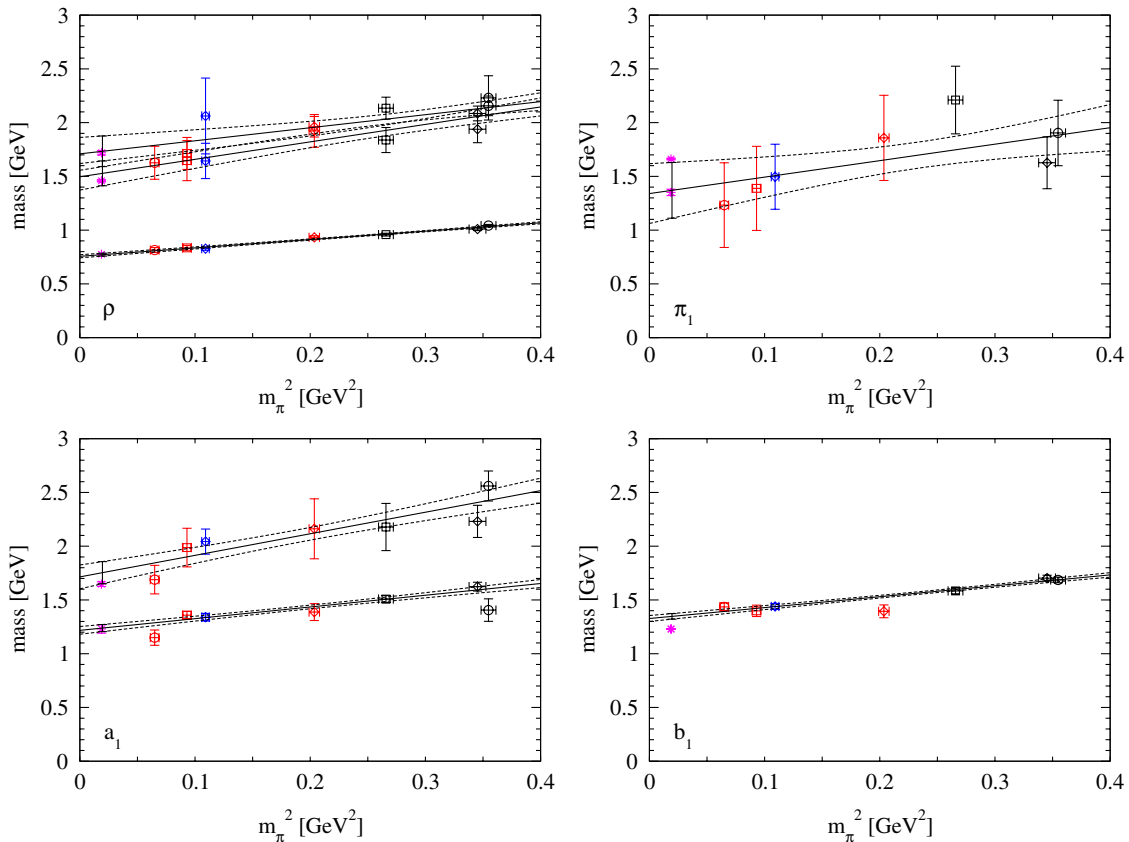


FIG. 6 (color online). (top left) $1^{--}(\rho)$; (top right) $1^{-+}(\pi_1)$; (bottom left) $1^{++}(\mathbf{a}_1)$; (bottom right) $1^{+-}(\mathbf{b}_1)$; for discussion refer to the text.

three interpolators out of (1, 2, 4, 13, 15, 17). Some of the plateaus tend to shift towards smaller masses at large time separations. However, as far as possible, long fit ranges are chosen. The chiral extrapolations hit the experimental $a_1(1260)$ and the $a_1(1640)$ within error bars (see Fig. 6).

$1^{+-}(\mathbf{b}_1)$: In the 1^{+-} channel, the ground state plateau is more stable than in its positive C -parity partner channel (a_1). Using the single interpolator (6), a mass with comparatively small error bar is obtained. The chiral extrapolation comes out too high, missing the experimental $b_1(1235)$ by more than 2σ (see Fig. 6).

C. Tensors

The continuum representation for spin 2 contributes to the irreducible representations T_2 and E on the lattice. These interpolators are orthogonal, thus masses can be extracted in each of them separately. In the continuum limit, the results should agree; however, at finite lattice spacings they can show different discretization effects. We extract the energy levels separately and compare the corresponding chiral extrapolations.

$2^{--}(\rho_2)$: In many of the spin 2 channels the signal is weak and fits can be performed only for some of the seven ensembles. In particular, this is the case in the 2^{--} channel

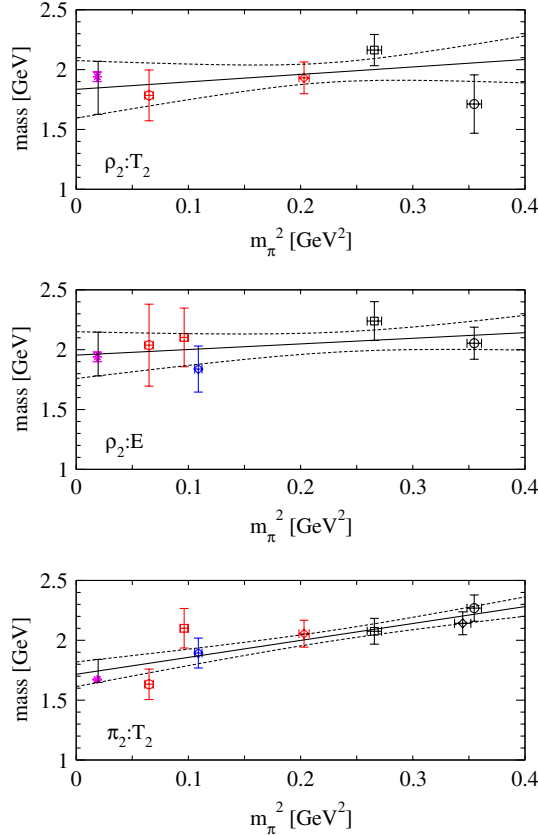


FIG. 7 (color online). (top and middle) 2^{--} (ρ_2) in both representations; (bottom) 2^{-+} (π_2) in representation T_2 .

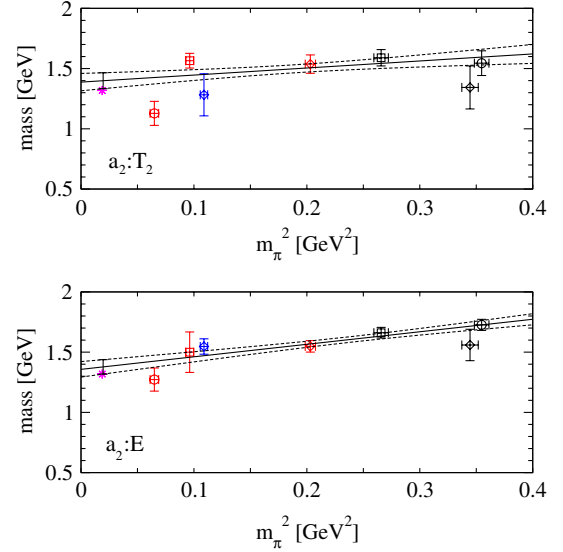


FIG. 8 (color online). 2^{++} (a_2) in both representations.

(see Fig. 7, top and middle). We use the single interpolator (2) in T_2 and also (2) in E . The effective masses are noisy, the fitted plateaus are rather short, with only 2 d.o.f. in the fits. Nevertheless, the chiral extrapolations of the T_2 and E ground state masses agree with each other and also with the experimental $\rho_2(1940)$ mass. Hence, our results are compatible with this state, which is omitted from the summary table of [36].

$2^{-+}(\pi_2)$: In the 2^{-+} channel (Fig. 7, bottom), interpolator (6) is applied in T_2 . The extrapolation to the physical point is compatible with the experimental $\pi_2(1670)$ (within 1, respectively 1.5σ). The signal for representation E (not shown) is too weak to be reliable.

2^{+-} : We studied this channel for completeness but the signals were inconclusive and did not allow to extract an energy level.

$2^{++}(a_2)$: In the 2^{++} channel (Fig. 8), we use interpolator (2) in T_2 and (2) [respectively (6) for A66] in E . Some of the plateaus are unexpectedly light, however, that might be statistical fluctuation. The chiral extrapolations of the T_2 and E ground state masses agree and both match the experimental $a_2(1320)$ mass within error bars. The $\chi^2/\text{d.o.f.}$ of the chiral fit of T_2 is larger than 3 (see Table IX), where the major contribution stems from ensemble A66. Finite volume effects could be responsible for the significant deviation of this particular value.

VI. MESONS WITH STRANGE VALENCE QUARKS

In 2-flavor simulations, strange hadrons can be studied by including the strange quark just as a valence quark. The corresponding quantum field theory is not well defined, the probability distribution of physical observables is not anymore strictly non-negative. Nevertheless, since the strange quark is heavy compared to the light,

dynamical quarks, observables can be measured and regarded as predictions including systematic errors. We stress that, even though light hadrons are well defined in 2-flavor simulations, they also show the systematic error of neglecting strange sea quarks when the results are compared to experiment. From this point of view, the predictive power of strange valence hadrons is not significantly below the one of light hadrons in 2-flavor simulations. The strange quark mass parameter is set in each ensemble such that the $\Omega(1672)$ is reproduced (always assuming that $r_{0,\text{exp}} = 0.48$ fm) (see Sec. III B).

In contrast to isovector light mesons, C -parity is no good quantum number for $I = \frac{1}{2}$ strange mesons due to the non-degeneracy of the light and strange quark mass. At unphysically large pion masses, however, C -parity is approximately restored. Our interpolators (see the Appendix) are constructed such that C -parity is a good quantum number in the limit of degenerate quark masses. Therefore, by monitoring the eigenvectors of the variational method, we can learn about the C -parity content of the states.

Since excited states are always more difficult to deal with than ground states, this raises the demands on the variational method. In some cases it is therefore suggestive to separate the channels according to C -parity. At our largest pion masses, around 600 MeV, one expects C -parity to be almost restored. Approaching the physical point, C -parity is violated stronger and stronger, and the corresponding mixing of interpolators is expected to become increasingly important. To investigate this mixing, we include all possible interpolators in the correlation matrix, but we also analyze separately the sectors with given C -parity. The advantage of the second approach is a clearer distinction of the energy levels, where some come in the $[C = +1]$ sector, some in the $[C = -1]$ sector. In the combined correlation matrix we see both sets, but due to the increased noise, fewer levels can be reliably determined. We discuss this point in the subsequent channels. Our results for the dominant C -parity assignments agree qualitatively with [2]. Here we also discuss the corresponding mixing, which is accessible due to our lighter pion masses.

A. Scalars

$(\mathbf{I} = \frac{1}{2}) \mathbf{0}^-(\mathbf{K})$: In the strange ($I = \frac{1}{2}$) 0^- channel, interpolator (1) is used for the ground state, which extrapolates close to the experimental kaon (see Fig. 9). The $\chi^2/\text{d.o.f.}$ of the chiral fit is larger than 4 (see Table X), which indicates that due to the tiny statistical errors the systematic errors (e.g. of setting the strange quark mass) become visible. For the excited state, we use the set (1, 2, 8, 17), its linear extrapolation agrees with the experimental $K(1460)$ within error bars. Hence, we can confirm this state (omitted from the summary table of [36]). In this channel we use only 0^{-+} interpolators, since the signal of the exotic 0^{--}

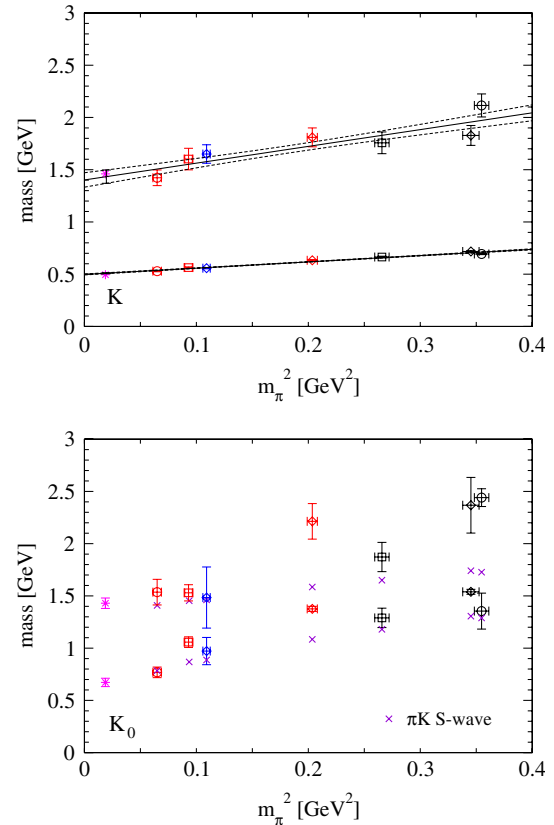


FIG. 9 (color online). (top) $(I = \frac{1}{2}) 0^-$ (K). (bottom) $(I = \frac{1}{2}) 0^+$ (K_0). The S-wave scattering state πK for zero and minimum nonzero relative momentum is indicated for all ensembles using crosses. The chiral fits are omitted for clarity.

interpolators is too weak, and the corresponding energy levels lie too high.

$(\mathbf{I} = \frac{1}{2}) \mathbf{0}^+(\mathbf{K}_0)$: The strange scalar channel 0^+ is as peculiar as its light multiplet partners. The $K_0^*(800)$ (also called κ) is a very broad resonance (with a width of more than 80% of its mass) and is omitted from the summary table of [36] due to its unclear nature.

Using interpolator (13) alone (not shown), the chiral extrapolation almost hits the presumed center of the resonance. To apply the variational method, we use the set (10, 12, 13) and include also (1, 4) in the basis at small pion masses. We observe that at light pion masses the effective masses tend to decrease at large time separations, which may be a signal for contributions of a scattering state. Like in most cases, we choose a large fit range (e.g., 8 time slices in A66). The results are compatible with the $K_0^*(800)$ and the $K_0^*(1430)$, but also with the S-wave scattering state πK (see Fig. 9). The $\chi^2/\text{d.o.f.}$ of the chiral fit of the ground state is larger than 8 (see Table X), which is again interpreted as indication for systematic errors, probably related to scattering states. Here we use only 0^{++} interpolators, the signal of the exotic 0^{+-} interpolators is too weak.

B. Vectors

($I = \frac{1}{2}$) $1^+(K^*)$: Considering the strange J^P channels as mixing of J^{P+} and J^{P-} , one can use information from the corresponding light J^{PC} channels to speculate about the dominating C -parity in the low-lying states of the strange J^P channel. Based on that analogy, in the scalar channels one expects dominance of positive C -parity, which is confirmed by our results. In the vector channels, however, both C -parities are expected to contribute to the measurable low-lying states. Looking at the experimental states in the corresponding light meson channels $\rho(770)$, $\pi_1(1300)$, $\rho(1450)$, and $\rho(1570$ or $1700)$, one expects that the $K^*(892)$ is an (almost) pure 1^{--} state, while mixing could become important for $K^*(1410)$ and $K^*(1680)$.

We first discuss sets of purely negative C -parity interpolators. Taking interpolators (1, 8, 12, 17, 20), we extract a ground state and up to two excitations. The chiral extrapolation of the ground state hits the experimental $K^*(892)$ nicely (see Fig. 10), which is clearly an (almost) pure $[C \approx -]$ state. The excitations are a bit high compared to the experimental $K^*(1410)$ and the $K^*(1680)$.

Considering only 1^{-+} interpolators, the chiral extrapolation hits the $K^*(1680)$. This suggests that mixing is important at least for the $K^*(1680)$.

Finally, taking the set (1, 8, 9, 12, 16, 20, 21), both types of C -parities are included in the variational method. In this analysis, the three lowest states are dominated by $[C \approx -]$ interpolators, where even for the excitations the mixing is compatible with zero. A slight mixing is observed in ensemble A66; however, the signal is very weak, and the corresponding energy levels cannot be extracted reliably. One might wonder why we do not see a significant contribution of $[C \approx +]$ interpolators to at least one of the excitations. A possible interpretation is that the mixing is indeed weak in this channel at all simulated pion masses and that there is a further state, dominated by $[C \approx +]$, which is not clearly identified in the full analysis. The chiral extrapolations of the excitations come out a bit high compared to the experimental $K^*(1410)$ and $K^*(1680)$, suggesting that simulations at smaller pion masses and with higher statistics are necessary in order to reliably describe the mixing of different C -parities and to be able to obtain the $K^*(1410)$.

($I = \frac{1}{2}$) $1^+(K_1)$: Looking at the experimental states in the corresponding light meson channels $a_1(1260)$, $b_1(1235)$ and $a_1(1640)$, mixing is expected already for the lowest states $K_1(1270)$, $K_1(1400)$, and $K_1(1650)$.

Employing pure $[C \approx +]$ sets of interpolators, the chiral extrapolation of the ground state ends up between the $K_1(1270)$ and the $K_1(1400)$. The first excitation hits the $K_1(1650)$ within error bars. From pure $[C \approx -]$ interpolators only a ground state can be extracted, the chiral extrapolation of which agrees with the $K_1(1400)$.

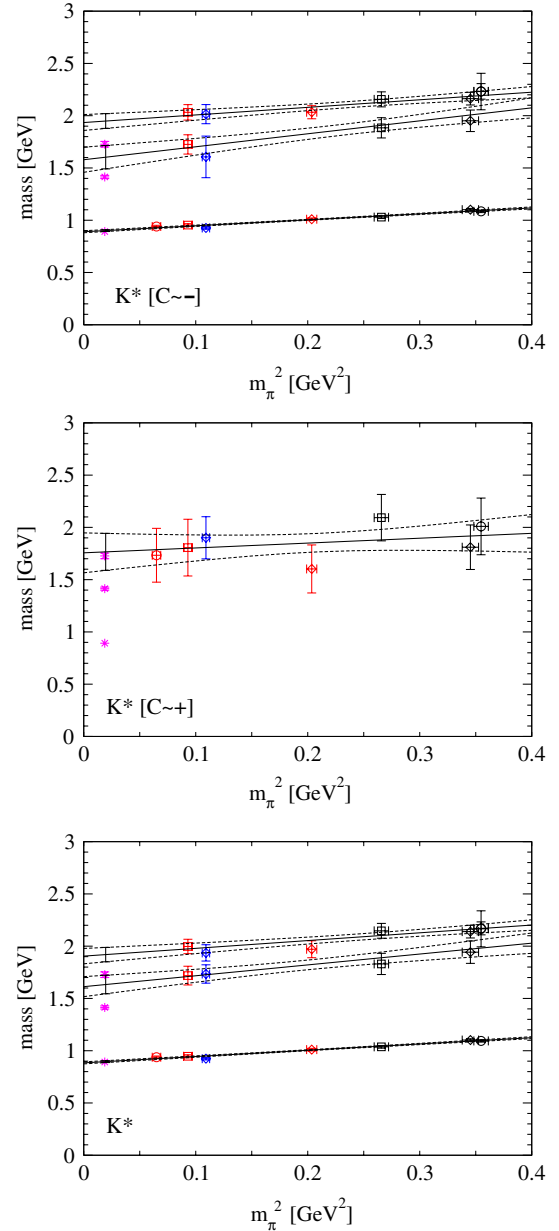


FIG. 10 (color online). ($I = \frac{1}{2}$) 1^- (K^*). Results for interpolators restricted to subsets with $[C \approx -]$ are shown on top and $[C \approx +]$ in the middle. Note that the ground state is missed in the $[C \approx +]$ subset. Results with both types are shown at the bottom.

Allowing for both types of C -parity, three states can be extracted when the set of interpolators is optimized in each ensemble. The chiral extrapolations are compatible with $K_1(1270)$, $K_1(1400)$, and $K_1(1650)$ (see Fig. 11). Since the splitting of $K_1(1270)$ and $K_1(1400)$ is rather small, it is hard to make a statement about its increase towards smaller pion masses. (Notice that an increased splitting is observed when mixing both charged conjugations for the analogous mesons in the charmed meson sector [54].) This is worsened by the fluctuation of the plateau points. However, the

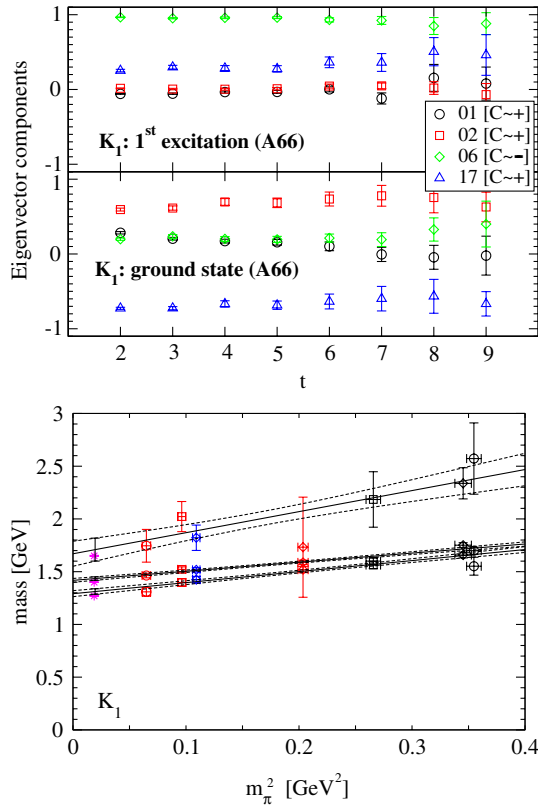


FIG. 11 (color online). 1^+ (K_1). Results for the energy levels are shown at the bottom. The corresponding eigenvectors for the ground state and the first excitation for the lightest pion mass (A66) are shown on top. Interpolators (1, 2, 17) have $[C \approx +]$, (6) has $[C \approx -]$. Note the dominance of positive (negative) C -parity in the ground state (first excitation). Note furthermore that there is some mixing in both states, which is allowed by the breaking of C -parity towards light pion masses. At our largest pion masses, this mixing is suppressed strongly.

eigenvectors indeed show stronger mixing approaching the physical point (see Fig. 11), which is usually accompanied by a more pronounced splitting. At simulated pion masses, $K_1(1270)$ and $K_1(1650)$ are dominated by $[C \approx +]$, $K_1(1400)$ by $[C \approx -]$ interpolators. Our results confirm the existence of $K_1(1650)$ (omitted from the summary table of [36]), which is dominated by positive C -parity in our analysis.

C. Tensors

($\mathbf{I} = \frac{1}{2}$) $2^-(\mathbf{K}_2)$: In the spin 2 channels, investigation of the mixing becomes more complicated, since the signal is often weak already for the ground state. From the light meson states $\pi_2(1670)$, $\pi_2(1880)$, and the (not established) $\rho_2(1940)$, one could expect a dominance of $[C \approx +]$ interpolators in the ground state. So far, $K_2(1580)$ is omitted from the summary table of [36], the lowest established states in this channel are $K_2(1770)$ and $K_2(1820)$.

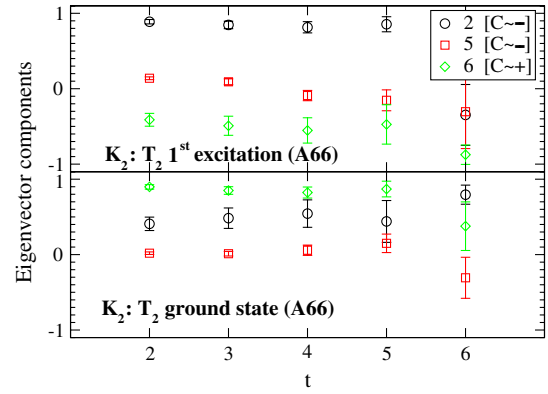


FIG. 12 (color online). ($I = \frac{1}{2}$) 2^- (K_2), representation T_2 : The eigenvectors for the ground state and the first excitation for the lightest pion mass (A66) are shown. Interpolators (2,5) have $[C \approx -]$, (6) has $[C \approx +]$. Note the dominance of positive (negative) C -parity in the ground state (first excitation). Note furthermore that there is significant mixing in both states, which is allowed by the breaking of C -parity towards light pion masses. At our largest pion masses, this mixing is suppressed. The mixing pattern is similar in representation E (not shown).

Restricting the basis to negative C -parity, we use interpolator (2) as in the corresponding light channel. In both T_2 and E , the chiral extrapolation is compatible with $K_2(1770)$ and $K_2(1820)$. For positive C -parity, using interpolator (6) in T_2 and (8) in E , the chiral extrapolations are again compatible with $K_2(1770)$ and $K_2(1820)$.

To take into account both C -parities, the set (2, 5, 6) [respectively (3, 4, 5, 6) in $C72$] is chosen in T_2 and (2, 5, 8) in E . The two lowest eigenvalues are very close and have to be sorted according to the eigenvectors. The eigenvectors of T_2 are shown in Fig. 12. We observe that the ground (excited) state is dominated by positive (negative) C -parity. However, there is significant mixing in both states, which appears to be the strongest mixing of all channels considered. Strong mixing is also observed in representation E . The chiral extrapolations are compatible with the experimentally established $K_2(1770)$ and $K_2(1820)$ (see upper panels of Fig. 13) and do not confirm the $K_2(1580)$, which is omitted from the summary table of [36]. However, increasing mixing towards lighter pion masses could still change the slope of the chiral extrapolation.

($\mathbf{I} = \frac{1}{2}$) $2^+(\mathbf{K}_2^*)$: No experimental state is known in the light-quark 2^{+-} channel. In the light 2^{++} channel, the lowest states are $a_2(1320)$, $a_2(1700)$, and $a_2(1950)$, of which the latter two are not established. In the strange 2^{+-} channel the lowest experimental states are $K_2^*(1430)$ and the (not established) $K_2^*(1980)$.

The signal of negative C -parity interpolators is weak here, thus we restrict our analysis to positive C -parity interpolators. Interpolator (2) (Table XI) is used in T_2

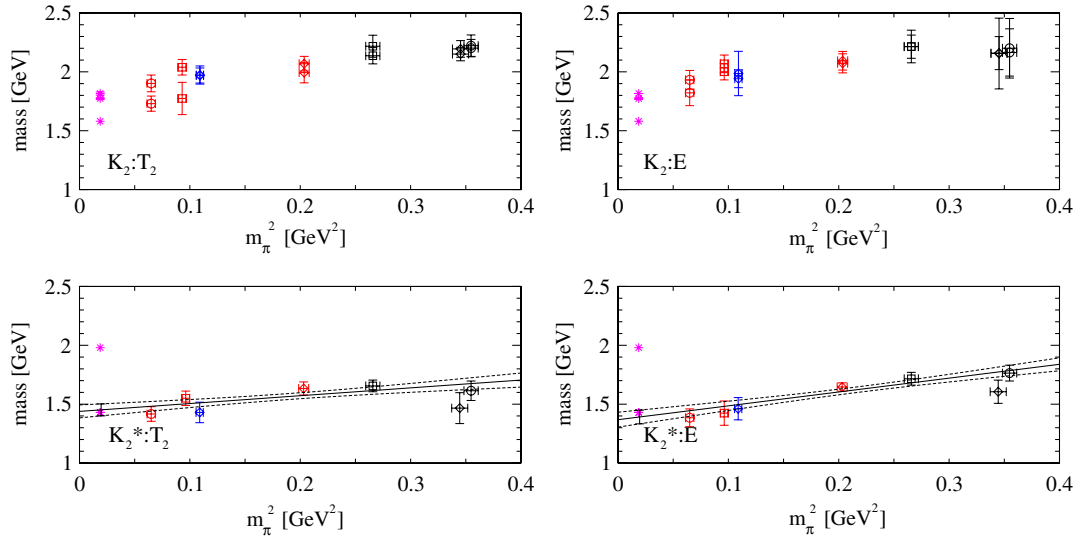


FIG. 13 (color online). Upper panels: $(I = \frac{1}{2}) 2^-$ (K_2) in both representations T_2 and E . Chiral fits are suppressed for clarity. Lower panels: $(I = \frac{1}{2}) 2^+$ in both representations T_2 and E (reliable signal only in $[C \approx +]$).

and interpolator (2) (Table IX) in E to extract a ground state mass. In both lattice channels, the chiral extrapolation hits the experimental $K_2^*(1430)$ nicely (see lower panels of Fig. 13).

D. Isoscalar light mesons

$1^{--}(\phi)$: In principle, correlation functions of isoscalar mesons include connected and disconnected diagrams. The low-lying isoscalar ϕ mesons decay mainly into kaons, thus one expects that these states are dominated by strange quarks (Zweig rule). Since disconnected diagrams are dominated by loops of light sea quarks, it is reasonable to assume that the ϕ mesons are dominated by connected (strange) diagrams. We extract ϕ meson masses evaluating only these connected diagrams, albeit with the systematic error of neglecting the disconnected diagrams. We use the same set of operators as in the light isovector 1^{--} (ρ) channel (Sec. VB) to extract three energy levels.

The ground state mass extrapolates to a value very close to the experimental $\phi(1020)$ mass (see Fig. 14), which confirms our choice of the strange quark mass parameters. The extrapolation of the excited states ends up significantly higher than the experimental $\phi(1680)$. Since the first excitation $\rho(1450)$ in the light isovector channel is reproduced nicely, one may conclude that the neglected disconnected diagrams play a more important role for the $\phi(1680)$ compared to the $\phi(1020)$. The lattice irreducible representation T_1 couples to continuum spins 1 and 3 (among others). This is why we also indicate the possible spin 3 state $\phi_3(1850)$ in the figure. This state is hit by the extrapolations of the first and second excitation. However, all our interpolators in this channel have a naive continuum limit of spin 1. One of

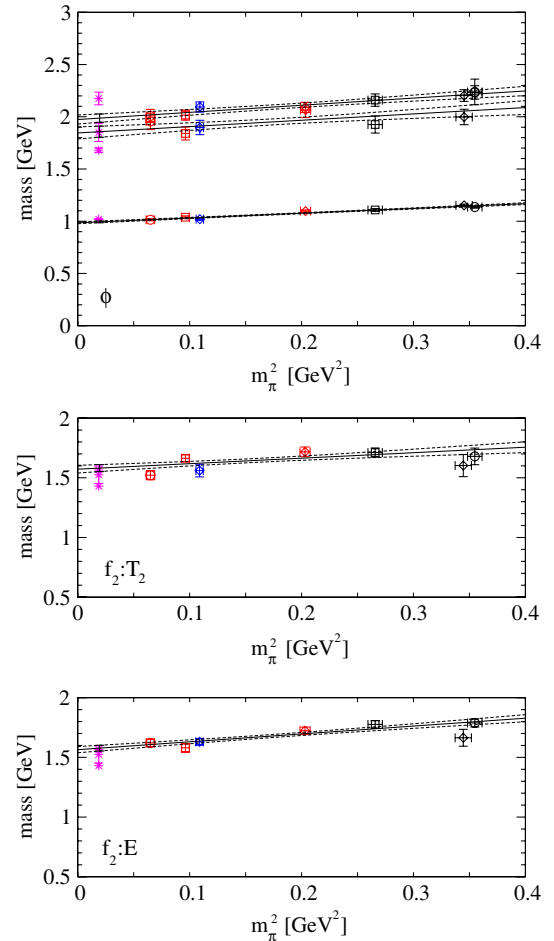


FIG. 14 (color online). (top) $(s\bar{s})1^{--}$; (middle and bottom) $(s\bar{s})2^{++}$.

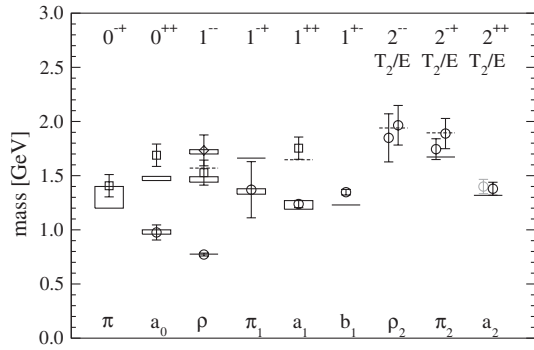


FIG. 15. Results for the isovector light meson masses. All values are obtained by chiral extrapolation linear in the pion mass squared. Horizontal lines or boxes represent experimentally known states, dashed lines indicate poor evidence, according to [36]. The statistical uncertainty of our results is indicated by bands of 1σ , that of the experimental values by boxes of 1σ . In case of spin 2 mesons, results for T_2 and E are shown side by side. Grey symbols denote a poor $\chi^2/\text{d.o.f.}$ of the chiral fits (see Table XII).

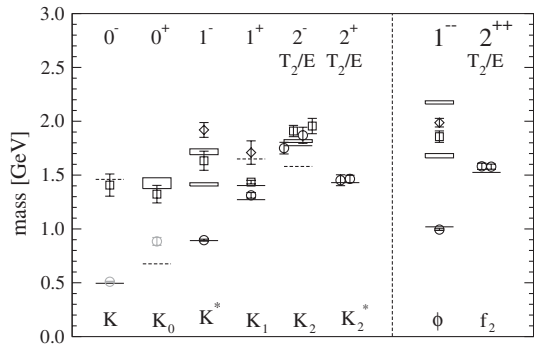


FIG. 16. Same as Fig. 15, but for strange mesons (left) and isoscalars (right). The strange quarks are implemented in the partial quenching approximation. The isoscalars additionally suffer from neglected disconnected diagrams. In the isoscalar sector we show experimental results only where they have a dominant $s\bar{s}$ content [36]. Grey symbols denote a poor $\chi^2/\text{d.o.f.}$ of the chiral fits (see Tables XIII and XIV).

these two levels may bend down if disconnected diagrams are included.

$2^{++}(\mathbf{f}_2)$: As in the ϕ meson channel, the experimental decay channels of the isoscalar light meson f_2 suggest dominance of connected diagrams. We use the same interpolators as in the isovector $2^{++}(a_2)$ channel. The results of T_2 and E agree (see Fig. 14), but their chiral extrapolations are in better agreement with the $f_2'(1525)$ than with the $f_2(1430)$. The latter needs confirmation and is not listed in the summary table of [36]. It is unclear if inclusion of the neglected disconnected diagrams would yield the $f_2(1430)$

or if the ground state of the theory is the established $f_2'(1525)$.

VII. CONCLUSIONS

We presented results for the light and strange meson spectrum from two dynamical Chirally Improved quarks. Seven ensembles with pion masses between 250 and 600 MeV were analyzed with the variational method in order to extract energy levels for ground and excited states. In addition to dynamical light quarks, we also included strange quarks within the partially quenched approximation, fitting the strange quark mass by requiring the correct $\Omega(1672)$ mass.

Figure 15 shows our chirally extrapolated results for the spectrum of light mesons compared to experimental values from [36]. Figure 16 contains a similar plot for strange mesons (left panel) and isoscalars (right panel). The results are in general in good agreement with experiment. For the strange mesons the good agreement for the ground states in the kaon, the K^* , and ϕ meson channels suggest that these observables are well reproduced in the partially quenched approximation and confirm our choice of strange quark mass parameter. As discussed in more detail in Secs. V and VI, we do not see any clear indications of scattering states, which probably show only little overlap with the one-particle interpolators used in this work. Exceptions are the strange 0^+ channel and the light isovector 0^+ channel at small quark masses, where our signal is also consistent with a two-particle scattering state.

The strange meson channels 1^- , 1^+ , and 2^- have been investigated with respect to their approximate C -parity. In the 1^- channel, the three lowest states seem to be dominated by negative C -parity, while positive C -parity was shown to contribute to a state in the vicinity of the second excitation. The 1^+ channel shows some mixing of different C -parity towards light pion masses, and the low-lying spectrum seems to contain states with alternating C -parity dominance. The 2^- channel shows strong mixing towards light pion masses and the ground state (first excitation) is dominated by positive (negative) C -parity.

For our lightest three pion masses finite size effects may play a non-negligible role and their influence on our results deserves further attention. A study on larger volumes is in progress and we will investigate this source of possible systematic errors in the near future. The larger volume will also be used for the spectroscopy of low-lying baryon states, where finite volume effects are expected to be more pronounced.

ACKNOWLEDGMENTS

We would like to thank Christof Gattringer and Leonid Y. Glozman for valuable discussions. The

calculations have been performed on the SGI Altix 4700 of the Leibniz-Rechenzentrum Munich and on local clusters at ZID at the University of Graz. We thank these institutions for providing support. M.L. has been supported by Austrian Science Fund (FWF: DK W1203-N16) and by EU FP7 project HadronPhysics2. D.M. acknowledges support by Natural Sciences and Engineering Research Council of Canada (NSERC) and G.P.E., M.L., and A.S. acknowledge support by the DFG Project No. SFB/TR-55.

APPENDIX: TABLES OF INTERPOLATORS

In the tables for meson interpolators (Tables IV, V, VI, VII, VIII, IX, X, and XI), the two quark fields are labeled by a and b . These are placeholders for light (u , d) or strange (s) quarks. The indices n , w , and ∂_i correspond to the smearings narrow, wide, and derivative, respectively. γ_i are the spatial Dirac matrices, γ_t is the Dirac matrix in time direction. ϵ_{ijk} is the Levi-Civita symbol, Q_{ijk} are Clebsch-Gordon coefficients, where all elements are zero except $Q_{111} = \frac{1}{\sqrt{2}}$, $Q_{122} = -\frac{1}{\sqrt{2}}$, $Q_{211} = -\frac{1}{\sqrt{6}}$, $Q_{222} = -\frac{1}{\sqrt{6}}$, and $Q_{233} = \frac{2}{\sqrt{6}}$.

TABLE IV. Meson interpolators for $J^P = 0^-$. The first row shows the number, the second shows the explicit form of the interpolator. In the last column the C -parity is given, which is only an approximate quantum number in the case of differing quark masses. Interpolators with different quark field smearings and similar Dirac structure are grouped and these groups separated by a horizontal rule.

# _{0⁻}	Interpolator	C
1	$\bar{a}_n \gamma_5 b_n$	+
2	$\bar{a}_n \gamma_5 b_w + \bar{a}_w \gamma_5 b_n$	+
3	$\bar{a}_n \gamma_5 b_w - \bar{a}_w \gamma_5 b_n$	-
4	$\bar{a}_w \gamma_5 b_w$	+
5	$\bar{a}_n \gamma_i \gamma_5 b_n$	+
6	$\bar{a}_n \gamma_i \gamma_5 b_w + \bar{a}_w \gamma_i \gamma_5 b_n$	+
7	$\bar{a}_n \gamma_i \gamma_5 b_w - \bar{a}_w \gamma_i \gamma_5 b_n$	-
8	$\bar{a}_w \gamma_i \gamma_5 b_w$	+
9	$\bar{a}_{\partial_i} \gamma_i \gamma_5 b_n + \bar{a}_n \gamma_i \gamma_5 b_{\partial_i}$	+
10	$\bar{a}_{\partial_i} \gamma_i \gamma_5 b_n - \bar{a}_n \gamma_i \gamma_5 b_{\partial_i}$	-
11	$\bar{a}_{\partial_i} \gamma_i \gamma_5 b_w + \bar{a}_w \gamma_i \gamma_5 b_{\partial_i}$	+
12	$\bar{a}_{\partial_i} \gamma_i \gamma_5 b_w - \bar{a}_w \gamma_i \gamma_5 b_{\partial_i}$	-
13	$\bar{a}_{\partial_i} \gamma_i \gamma_t \gamma_5 b_n + \bar{a}_n \gamma_i \gamma_t \gamma_5 b_{\partial_i}$	-
14	$\bar{a}_{\partial_i} \gamma_i \gamma_t \gamma_5 b_n - \bar{a}_n \gamma_i \gamma_t \gamma_5 b_{\partial_i}$	+
15	$\bar{a}_{\partial_i} \gamma_i \gamma_t \gamma_5 b_w + \bar{a}_w \gamma_i \gamma_t \gamma_5 b_{\partial_i}$	-
16	$\bar{a}_{\partial_i} \gamma_i \gamma_t \gamma_5 b_w - \bar{a}_w \gamma_i \gamma_t \gamma_5 b_{\partial_i}$	+
17	$\bar{a}_{\partial_i} \gamma_5 b_{\partial_i}$	+
18	$\bar{a}_{\partial_i} \gamma_t \gamma_5 b_{\partial_i}$	+

TABLE V. Same as Table IV, now for $J^P = 0^+$.

# _{0⁺}	Interpolator(s)	C -parity
1	$\bar{a}_n b_n$	+
2	$\bar{a}_n b_w + \bar{a}_w b_n$	+
3	$\bar{a}_n b_w - \bar{a}_w b_n$	-
4	$\bar{a}_w b_w$	+
5	$\bar{a}_{\partial_i} \gamma_i b_n + \bar{a}_n \gamma_i b_{\partial_i}$	-
6	$\bar{a}_{\partial_i} \gamma_i b_n - \bar{a}_n \gamma_i b_{\partial_i}$	+
7	$\bar{a}_{\partial_i} \gamma_i b_w + \bar{a}_w \gamma_i b_{\partial_i}$	-
8	$\bar{a}_{\partial_i} \gamma_i b_w - \bar{a}_w \gamma_i b_{\partial_i}$	+
9	$\bar{a}_{\partial_i} \gamma_i \gamma_t b_n + \bar{a}_n \gamma_i \gamma_t b_{\partial_i}$	-
10	$\bar{a}_{\partial_i} \gamma_i \gamma_t b_n - \bar{a}_n \gamma_i \gamma_t b_{\partial_i}$	+
11	$\bar{a}_{\partial_i} \gamma_i \gamma_t b_w + \bar{a}_w \gamma_i \gamma_t b_{\partial_i}$	-
12	$\bar{a}_{\partial_i} \gamma_i \gamma_t b_w - \bar{a}_w \gamma_i \gamma_t b_{\partial_i}$	+
13	$\bar{a}_{\partial_i} b_{\partial_i}$	+

TABLE VI. Same as Table IV, now for $J^P = 1^-$.

# _{1⁻}	Interpolator(s)	C
1	$\bar{a}_n \gamma_k b_n$	-
2	$\bar{a}_n \gamma_k b_w + \bar{a}_w \gamma_k b_n$	-
3	$\bar{a}_n \gamma_k b_w - \bar{a}_w \gamma_k b_n$	+
4	$\bar{a}_w \gamma_k b_w$	-
5	$\bar{a}_n \gamma_k \gamma_t b_n$	-
6	$\bar{a}_n \gamma_k \gamma_t b_w + \bar{a}_w \gamma_k \gamma_t b_n$	-
7	$\bar{a}_n \gamma_k \gamma_t b_w - \bar{a}_w \gamma_k \gamma_t b_n$	+
8	$\bar{a}_w \gamma_k \gamma_t b_w$	-
9	$\bar{a}_{\partial_k} b_n + \bar{a}_n b_{\partial_k}$	+
10	$\bar{a}_{\partial_k} b_n - \bar{a}_n b_{\partial_k}$	-
11	$\bar{a}_{\partial_k} b_w + \bar{a}_w b_{\partial_k}$	+
12	$\bar{a}_{\partial_k} b_w - \bar{a}_w b_{\partial_k}$	-
13	$\bar{a}_{\partial_k} \gamma_t b_n + \bar{a}_n \gamma_t b_{\partial_k}$	-
14	$\bar{a}_{\partial_k} \gamma_t b_n - \bar{a}_n \gamma_t b_{\partial_k}$	+
15	$\bar{a}_{\partial_k} \gamma_t b_w + \bar{a}_w \gamma_t b_{\partial_k}$	-
16	$\bar{a}_{\partial_k} \gamma_t b_w - \bar{a}_w \gamma_t b_{\partial_k}$	+
17	$\bar{a}_{\partial_i} \gamma_k b_{\partial_i}$	-
18	$\bar{a}_{\partial_i} \gamma_k \gamma_t b_{\partial_i}$	-
19	$\bar{a}_{\partial_k} \epsilon_{ijk} \gamma_j \gamma_5 b_n + \bar{a}_n \epsilon_{ijk} \gamma_j \gamma_5 b_{\partial_k}$	+
20	$\bar{a}_{\partial_k} \epsilon_{ijk} \gamma_j \gamma_5 b_n - \bar{a}_n \epsilon_{ijk} \gamma_j \gamma_5 b_{\partial_k}$	-
21	$\bar{a}_{\partial_k} \epsilon_{ijk} \gamma_j \gamma_5 b_w + \bar{a}_w \epsilon_{ijk} \gamma_j \gamma_5 b_{\partial_k}$	+
22	$\bar{a}_{\partial_k} \epsilon_{ijk} \gamma_j \gamma_5 b_w - \bar{a}_w \epsilon_{ijk} \gamma_j \gamma_5 b_{\partial_k}$	-
23	$\bar{a}_{\partial_k} \epsilon_{ijk} \gamma_j \gamma_t \gamma_5 b_n + \bar{a}_n \epsilon_{ijk} \gamma_j \gamma_t \gamma_5 b_{\partial_k}$	-
24	$\bar{a}_{\partial_k} \epsilon_{ijk} \gamma_j \gamma_t \gamma_5 b_n - \bar{a}_n \epsilon_{ijk} \gamma_j \gamma_t \gamma_5 b_{\partial_k}$	+
25	$\bar{a}_{\partial_k} \epsilon_{ijk} \gamma_j \gamma_t \gamma_5 b_w + \bar{a}_w \epsilon_{ijk} \gamma_j \gamma_t \gamma_5 b_{\partial_k}$	-
26	$\bar{a}_{\partial_k} \epsilon_{ijk} \gamma_j \gamma_t \gamma_5 b_w - \bar{a}_w \epsilon_{ijk} \gamma_j \gamma_t \gamma_5 b_{\partial_k}$	+

TABLE VII. Same as Table IV, now for $J^P = 1^+$.

# _{1⁺}	Interpolator(s)	C
1	$\bar{a}_n \gamma_k \gamma_5 b_n$	+
2	$\bar{a}_n \gamma_k \gamma_5 b_w + \bar{a}_w \gamma_k \gamma_5 b_n$	+
3	$\bar{a}_n \gamma_k \gamma_5 b_w - \bar{a}_w \gamma_k \gamma_5 b_n$	-
4	$\bar{a}_w \gamma_k \gamma_5 b_w$	+
5	$\bar{a}_{\partial_k} \gamma_5 b_n + \bar{a}_n \gamma_5 b_{\partial_k}$	+
6	$\bar{a}_{\partial_k} \gamma_5 b_n - \bar{a}_n \gamma_5 b_{\partial_k}$	-
7	$\bar{a}_{\partial_k} \gamma_5 b_w + \bar{a}_w \gamma_5 b_{\partial_k}$	+
8	$\bar{a}_{\partial_k} \gamma_5 b_w - \bar{a}_w \gamma_5 b_{\partial_k}$	-
9	$\bar{a}_{\partial_k} \gamma_i \gamma_5 b_n + \bar{a}_n \gamma_i \gamma_5 b_{\partial_k}$	+
10	$\bar{a}_{\partial_k} \gamma_i \gamma_5 b_n - \bar{a}_n \gamma_i \gamma_5 b_{\partial_k}$	-
11	$\bar{a}_{\partial_k} \gamma_i \gamma_5 b_w + \bar{a}_w \gamma_i \gamma_5 b_{\partial_k}$	+
12	$\bar{a}_{\partial_k} \gamma_i \gamma_5 b_w - \bar{a}_w \gamma_i \gamma_5 b_{\partial_k}$	-
13	$\bar{a}_{\partial_i} \gamma_k \gamma_5 b_{\partial_i}$	+
14	$\epsilon_{ijk} \bar{a}_{\partial_k} \gamma_j b_n + \epsilon_{ijk} \bar{a}_n \gamma_j b_{\partial_k}$	-
15	$\epsilon_{ijk} \bar{a}_{\partial_k} \gamma_j b_n - \epsilon_{ijk} \bar{a}_n \gamma_j b_{\partial_k}$	+
16	$\epsilon_{ijk} \bar{a}_{\partial_k} \gamma_j b_w + \epsilon_{ijk} \bar{a}_w \gamma_j b_{\partial_k}$	-
17	$\epsilon_{ijk} \bar{a}_{\partial_k} \gamma_j b_w - \epsilon_{ijk} \bar{a}_w \gamma_j b_{\partial_k}$	+
18	$\epsilon_{ijk} \bar{a}_{\partial_k} \gamma_j \gamma_t b_n + \epsilon_{ijk} \bar{a}_n \gamma_j \gamma_t b_{\partial_k}$	-
19	$\epsilon_{ijk} \bar{a}_{\partial_k} \gamma_j \gamma_t b_n - \epsilon_{ijk} \bar{a}_n \gamma_j \gamma_t b_{\partial_k}$	+
20	$\epsilon_{ijk} \bar{a}_{\partial_k} \gamma_j \gamma_t b_w + \epsilon_{ijk} \bar{a}_w \gamma_j \gamma_t b_{\partial_k}$	-
21	$\epsilon_{ijk} \bar{a}_{\partial_k} \gamma_j \gamma_t b_w - \epsilon_{ijk} \bar{a}_w \gamma_j \gamma_t b_{\partial_k}$	+
22	$\bar{a}_n \gamma_k \gamma_t \gamma_5 b_n$	-
23	$\bar{a}_n \gamma_k \gamma_t \gamma_5 b_w + \bar{a}_w \gamma_k \gamma_t \gamma_5 b_n$	-
24	$\bar{a}_n \gamma_k \gamma_t \gamma_5 b_w - \bar{a}_w \gamma_k \gamma_t \gamma_5 b_n$	+
25	$\bar{a}_w \gamma_k \gamma_t \gamma_5 b_w$	-
26	$\bar{a}_{\partial_i} \gamma_k \gamma_t \gamma_5 b_{\partial_i}$	-

TABLE VIII. Same as Table IV, now for $J^P = 2^- E$.

# _{2⁻E}	Interpolator(s)	C
1	$Q_{ijk} \bar{a}_{\partial_k} \gamma_j \gamma_t \gamma_5 b_n + Q_{ijk} \bar{a}_n \gamma_j \gamma_t \gamma_5 b_{\partial_k}$	-
2	$Q_{ijk} \bar{a}_{\partial_k} \gamma_j \gamma_t \gamma_5 b_n - Q_{ijk} \bar{a}_n \gamma_j \gamma_t \gamma_5 b_{\partial_k}$	+
3	$Q_{ijk} \bar{a}_{\partial_k} \gamma_j \gamma_t \gamma_5 b_w + Q_{ijk} \bar{a}_w \gamma_j \gamma_t \gamma_5 b_{\partial_k}$	-
4	$Q_{ijk} \bar{a}_{\partial_k} \gamma_j \gamma_t \gamma_5 b_w - Q_{ijk} \bar{a}_w \gamma_j \gamma_t \gamma_5 b_{\partial_k}$	+
5	$Q_{ijk} \bar{a}_{\partial_j} \gamma_5 b_{\partial_k}$	+
6	$Q_{ijk} \bar{a}_{\partial_j} \gamma_t \gamma_5 b_{\partial_k}$	+
7	$Q_{ijk} \bar{a}_{\partial_k} \gamma_j \gamma_5 b_n + Q_{ijk} \bar{a}_n \gamma_j \gamma_5 b_{\partial_k}$	+
8	$Q_{ijk} \bar{a}_{\partial_k} \gamma_j \gamma_5 b_n - Q_{ijk} \bar{a}_n \gamma_j \gamma_5 b_{\partial_k}$	-
9	$Q_{ijk} \bar{a}_{\partial_k} \gamma_j \gamma_5 b_w + Q_{ijk} \bar{a}_w \gamma_j \gamma_5 b_{\partial_k}$	+
10	$Q_{ijk} \bar{a}_{\partial_k} \gamma_j \gamma_5 b_w - Q_{ijk} \bar{a}_w \gamma_j \gamma_5 b_{\partial_k}$	-

TABLE IX. Same as Table IV, now for $J^P = 2^+ E$.

# _{2⁺E}	Interpolator(s)	C
1	$Q_{ijk} \bar{a}_{\partial_k} \gamma_j b_n + Q_{ijk} \bar{a}_n \gamma_j b_{\partial_k}$	-
2	$Q_{ijk} \bar{a}_{\partial_k} \gamma_j b_n - Q_{ijk} \bar{a}_n \gamma_j b_{\partial_k}$	+
3	$Q_{ijk} \bar{a}_{\partial_k} \gamma_j b_w + Q_{ijk} \bar{a}_w \gamma_j b_{\partial_k}$	-
4	$Q_{ijk} \bar{a}_{\partial_k} \gamma_j b_w - Q_{ijk} \bar{a}_w \gamma_j b_{\partial_k}$	+
5	$Q_{ijk} \bar{a}_{\partial_k} \gamma_j \gamma_t b_n + Q_{ijk} \bar{a}_n \gamma_j \gamma_t b_{\partial_k}$	-
6	$Q_{ijk} \bar{a}_{\partial_k} \gamma_j \gamma_t b_n - Q_{ijk} \bar{a}_n \gamma_j \gamma_t b_{\partial_k}$	+
7	$Q_{ijk} \bar{a}_{\partial_k} \gamma_j \gamma_t b_w + Q_{ijk} \bar{a}_w \gamma_j \gamma_t b_{\partial_k}$	-
8	$Q_{ijk} \bar{a}_{\partial_k} \gamma_j \gamma_t b_w - Q_{ijk} \bar{a}_w \gamma_j \gamma_t b_{\partial_k}$	+
9	$Q_{ijk} \bar{a}_{\partial_j} b_{\partial_k}$	+
10	$Q_{ijk} \bar{a}_{\partial_j} \gamma_t b_{\partial_k}$	-

TABLE X. Same as Table IV, now for $J^P = 2^- T_2$.

# _{2⁻T₂}	Interpolator(s)	C
1	$ \epsilon_{ijk} \bar{a}_{\partial_k} \gamma_j \gamma_5 b_n + \epsilon_{ijk} \bar{a}_n \gamma_j \gamma_5 b_{\partial_k}$	+
2	$ \epsilon_{ijk} \bar{a}_{\partial_k} \gamma_j \gamma_5 b_n - \epsilon_{ijk} \bar{a}_n \gamma_j \gamma_5 b_{\partial_k}$	-
3	$ \epsilon_{ijk} \bar{a}_{\partial_k} \gamma_j \gamma_5 b_w + \epsilon_{ijk} \bar{a}_w \gamma_j \gamma_5 b_{\partial_k}$	+
4	$ \epsilon_{ijk} \bar{a}_{\partial_k} \gamma_j \gamma_5 b_w - \epsilon_{ijk} \bar{a}_w \gamma_j \gamma_5 b_{\partial_k}$	-
5	$ \epsilon_{ijk} \bar{a}_{\partial_k} \gamma_j \gamma_t \gamma_5 b_n + \epsilon_{ijk} \bar{a}_n \gamma_j \gamma_t \gamma_5 b_{\partial_k}$	-
6	$ \epsilon_{ijk} \bar{a}_{\partial_k} \gamma_j \gamma_t \gamma_5 b_n - \epsilon_{ijk} \bar{a}_n \gamma_j \gamma_t \gamma_5 b_{\partial_k}$	+
7	$ \epsilon_{ijk} \bar{a}_{\partial_k} \gamma_j \gamma_t \gamma_5 b_w + \epsilon_{ijk} \bar{a}_w \gamma_j \gamma_t \gamma_5 b_{\partial_k}$	-
8	$ \epsilon_{ijk} \bar{a}_{\partial_k} \gamma_j \gamma_t \gamma_5 b_w - \epsilon_{ijk} \bar{a}_w \gamma_j \gamma_t \gamma_5 b_{\partial_k}$	+

TABLE XI. Same as Table IV, now for $J^P = 2^+ T_2$.

# _{2⁺T₂}	Interpolator(s)	C
1	$ \epsilon_{ijk} \bar{a}_{\partial_k} \gamma_j b_n + \epsilon_{ijk} \bar{a}_n \gamma_j b_{\partial_k}$	-
2	$ \epsilon_{ijk} \bar{a}_{\partial_k} \gamma_j b_n - \epsilon_{ijk} \bar{a}_n \gamma_j b_{\partial_k}$	+
3	$ \epsilon_{ijk} \bar{a}_{\partial_k} \gamma_j b_w + \epsilon_{ijk} \bar{a}_w \gamma_j b_{\partial_k}$	-
4	$ \epsilon_{ijk} \bar{a}_{\partial_k} \gamma_j b_w - \epsilon_{ijk} \bar{a}_w \gamma_j b_{\partial_k}$	+
5	$ \epsilon_{ijk} \bar{a}_{\partial_k} \gamma_j \gamma_t b_n + \epsilon_{ijk} \bar{a}_n \gamma_j \gamma_t b_{\partial_k}$	-
6	$ \epsilon_{ijk} \bar{a}_{\partial_k} \gamma_j \gamma_t b_n - \epsilon_{ijk} \bar{a}_n \gamma_j \gamma_t b_{\partial_k}$	+
7	$ \epsilon_{ijk} \bar{a}_{\partial_k} \gamma_j \gamma_t b_w + \epsilon_{ijk} \bar{a}_w \gamma_j \gamma_t b_{\partial_k}$	-
8	$ \epsilon_{ijk} \bar{a}_{\partial_k} \gamma_j \gamma_t b_w - \epsilon_{ijk} \bar{a}_w \gamma_j \gamma_t b_{\partial_k}$	+

TABLE XII. Energy levels at the physical point and corresponding $\chi^2/\text{d.o.f.}$ for the chiral fits of the isovector light meson energy levels reported in this work. Sources of large $\chi^2/\text{d.o.f.}$ (≥ 3) are discussed in the text.

Light meson	Energy level [MeV]	$\chi^2/\text{d.o.f.}$
0^{-+}	1407(103)	8.25/5
0^{++}	976(70)	12.38/5
0^{++}	1689(103)	6.70/4
1^{--}	772(13)	4.65/5
1^{--}	1528(115)	2.79/5
1^{--}	1733(143)	2.51/4
1^{-+}	1370(260)	3.78/5
1^{+-}	1347(26)	8.12/5
1^{++}	1238(33)	9.62/5
1^{++}	1754(103)	4.91/5
$2^{--}(T_2)$	1849(222)	3.77/2
$2^{--}(E)$	1965(183)	2.16/3
$2^{-+}(T_2)$	1745(96)	5.06/5
$2^{-+}(E)$	1889(139)	8.96/4
$2^{++}(T_2)$	1399(66)	16.51/5
$2^{++}(E)$	1379(60)	6.03/5

TABLE XIII. Same as Table XII, but for strange mesons.

Strange meson	Energy level [MeV]	$\chi^2/\text{d.o.f.}$
0^{-}	509(4)	20.83/5
0^{-}	1434(64)	6.94/5
0^{+}	884(36)	41.53/5
0^{+}	1323(81)	6.92/5
1^{-}	896(9)	7.20/5
1^{-}	1633(89)	1.57/3
1^{-}	1919(69)	1.05/3
1^{+}	1339(20)	3.90/5
1^{+}	1409(17)	6.76/5
1^{+}	1709(109)	2.56/5
$2^{-}(T_2)$	1750(54)	5.31/5
$2^{-}(T_2)$	1909(52)	2.21/5
$2^{-}(E)$	1870(75)	1.51/4
$2^{-}(E)$	1956(71)	1.17/4
$2^{+}(T_2)$	1452(51)	7.28/5
$2^{+}(E)$	1392(58)	5.68/5

TABLE XIV. Same as Table XII, but for isoscalar mesons.

Isoscalar meson	Energy level [MeV]	$\chi^2/\text{d.o.f.}$
1^{--}	994(8)	6.51/5
1^{--}	1857(53)	7.30/5
1^{--}	1987(40)	1.41/5
$2^{++}(T_2)$	1581(29)	12.89/5
$2^{++}(E)$	1578(24)	7.28/5

- [1] G. P. Engel, C. B. Lang, M. Limmer, D. Mohler, and A. Schäfer (BGR [Bern-Graz-Regensburg] Collaboration), *Phys. Rev. D* **82**, 034505 (2010).
- [2] J. J. Dudek, R. G. Edwards, M. J. Peardon, D. G. Richards, and C. E. Thomas, *Phys. Rev. D* **82**, 034508 (2010).
- [3] J. Foley *et al.*, *Comput. Phys. Commun.* **172**, 145 (2005).
- [4] M. Peardon, J. Bulava, J. Foley, C. Morningstar, J. Dudek, R. G. Edwards, B. Joo, H.-W. Lin, D. G. Richards, and K. J. Juge (Hadron Spectrum Collaboration), *Phys. Rev. D* **80**, 054506 (2009).
- [5] C. Morningstar, J. Bulava, J. Foley, K. J. Juge, D. Lenkner, M. Peardon, and C. H. Wong, *Phys. Rev. D* **83**, 114505 (2011).
- [6] G. S. Bali, S. Collins, and A. Schaefer, *Comput. Phys. Commun.* **181**, 1570 (2010).
- [7] G. Bali, L. Castagnini, and S. Collins, Proc. Sci., LATTICE2010 (2010) 096.
- [8] R. G. Petry, D. Harnett, R. Lewis, and R. M. Woloshyn, *Phys. Rev. D* **78**, 074502 (2008).
- [9] T. Burch, C. Hagen, M. Hetzenegger, and A. Schäfer, *Phys. Rev. D* **79**, 114503 (2009).
- [10] G. T. Fleming, S. D. Cohen, H. W. Lin, and V. Pereyra, *Phys. Rev. D* **80**, 074506 (2009).
- [11] J. J. Dudek, R. G. Edwards, M. J. Peardon, D. G. Richards, and C. E. Thomas, *Phys. Rev. Lett.* **103**, 262001 (2009).
- [12] J. J. Dudek, R. G. Edwards, B. Joo, M. J. Peardon, D. G. Richards, and C. E. Thomas, *Phys. Rev. D* **83**, 111502 (2011).
- [13] C. Morningstar, A. Bell, J. Bulava, J. Foley, K. J. Juge, D. Lenkner, and C. Wong, *AIP Conf. Proc.* **1388**, 34 (2011).
- [14] M. Lüscher and U. Wolff, *Nucl. Phys.* **B339**, 222 (1990).
- [15] C. Michael, *Nucl. Phys.* **B259**, 58 (1985).
- [16] A. Krassnigg, *Phys. Rev. D* **80**, 114010 (2009).
- [17] M. Blank, A. Krassnigg, and A. Maas, *Phys. Rev. D* **83**, 034020 (2011).
- [18] A. Krassnigg and M. Blank, *Phys. Rev. D* **83**, 096006 (2011).
- [19] J. R. Pelaez and G. Rios, *Phys. Rev. D* **82**, 114002 (2010).
- [20] V. Bernard, M. Lage, U. G. Meissner, and A. Rusetsky, *J. High Energy Phys.* **01** (2011) 019.
- [21] M. Döring, U.-G. Meißner, E. Oset, and A. Rusetsky, *Eur. Phys. J. A* **47**, 139 (2011).
- [22] M. Döring and U.-G. Meißner, *J. High Energy Phys.* **01** (2012) 009.
- [23] C. Gattringer, C. Hagen, C. B. Lang, M. Limmer, D. Mohler, and A. Schäfer, *Phys. Rev. D* **79**, 054501 (2009).
- [24] C. Gattringer, *Phys. Rev. D* **63**, 114501 (2001).
- [25] C. Gattringer, I. Hip, and C. B. Lang, *Nucl. Phys.* **B597**, 451 (2001).
- [26] G. P. Engel, C. B. Lang, M. Limmer, D. Mohler, and A. Schäfer, Proc. Sci., Lattice 2011 (2011) 119.
- [27] C. Morningstar and M. Peardon, *Phys. Rev. D* **69**, 054501 (2004).
- [28] M. Lüscher and P. Weisz, *Commun. Math. Phys.* **97**, 59 (1985).
- [29] C. Gattringer, M. Göckeler, P. Hasenfratz, S. Hauswirth, K. Holland, T. Jörg, K. J. Juge, C. B. Lang, F. Niedermayer, P. E. L. Rakow, S. Schaefer, and A. Schäfer, *Nucl. Phys.* **B677**, 3 (2004).

- [30] S. Dürr, Z. Fodor, J. Frison, C. Hoelbling, R. Hoffmann, S. Katz, S. Krieg, T. Kurth, L. Lellouch, T. Lippert, K. Szabo, and G. Vulvert, *Science* **322**, 1224 (2008).
- [31] P. Huber, *J. High Energy Phys.* 11 (2010) 107.
- [32] T. Maurer, Ph.D. thesis, University of Regensburg, Germany, 2011.
- [33] J. Gasser and H. Leutwyler, *Ann. Phys. (N.Y.)* **158**, 142 (1984).
- [34] G. Colangelo, J. Gasser, and H. Leutwyler, *Nucl. Phys. B* **603**, 125 (2001).
- [35] J. Bijnens, Proc. Sci., LATTICE2007 (2007) 004.
- [36] K. Nakamura *et al.*, *J. Phys. G* **37**, 075021 (2010).
- [37] B. Blossier, M. DellaMorte, G. von Hippel, T. Mendes, and R. Sommer, *J. High Energy Phys.* 04 (2009) 094.
- [38] T. Burch, C. Gattringer, L. Y. Glozman, C. Hagen, and C. B. Lang, *Phys. Rev. D* **73**, 017502 (2006).
- [39] T. Burch, C. Gattringer, L. Y. Glozman, R. Kleindl, C. B. Lang, and A. Schäfer, *Phys. Rev. D* **70**, 054502 (2004).
- [40] X. Liao and T. Manke, [arXiv:hep-lat/0210030](https://arxiv.org/abs/hep-lat/0210030).
- [41] J.J. Dudek, R.G. Edwards, N. Mathur, and D.G. Richards, *Phys. Rev. D* **77**, 034501 (2008).
- [42] C. Gattringer, L. Y. Glozman, C. B. Lang, D. Mohler, and S. Prelovsek, *Phys. Rev. D* **78**, 034501 (2008).
- [43] T. Burch, C. Gattringer, L. Y. Glozman, C. Hagen, D. Hierl, C. B. Lang, and A. Schäfer, *Phys. Rev. D* **74**, 014504 (2006).
- [44] T. Burch, C. Gattringer, L. Y. Glozman, C. Hagen, C. B. Lang, and A. Schäfer, *Phys. Rev. D* **73**, 094505 (2006).
- [45] A. Hasenfratz, R. Hoffmann, and F. Knechtli, *Nucl. Phys. B, Proc. Suppl.* **106**, 418 (2002).
- [46] A. Hasenfratz and F. Knechtli, *Phys. Rev. D* **64**, 034504 (2001).
- [47] A. Hasenfratz, R. Hoffmann, and S. Schaefer, *J. High Energy Phys.* 05 (2007) 029.
- [48] S. Güsken *et al.*, *Phys. Lett. B* **227**, 266 (1989).
- [49] C. Best, M. Göckeler, R. Horsley, E.-M. Ilgenfritz, H. Perlt, P. Rakow, A. Schäfer, G. Schierholz, A. Schiller, and S. Schramm, *Phys. Rev. D* **56**, 2743 (1997).
- [50] C. Gattringer, C. B. Lang, M. Limmer, T. Maurer, D. Mohler, and A. Schäfer, Proc. Sci., LATTICE 2008 (2008) 093.
- [51] S. Prelovsek, T. Draper, C. B. Lang, M. Limmer, K.-F. Liu, N. Mathur, and D. Mohler, *Phys. Rev. D* **82**, 094507 (2010).
- [52] J. Bulava *et al.*, *Phys. Rev. D* **82**, 014507 (2010).
- [53] C. B. Lang, D. Mohler, S. Prelovsek, and M. Vidmar, *Phys. Rev. D* **84**, 054503 (2011).
- [54] D. Mohler and R. Woloshyn, *Phys. Rev. D* **84**, 054505 (2011).